Analyst

PAPER

View Article Online
View Journal | View Issue

Cite this: *Analyst*, 2018, **143**, 429

A reversible fluorescent probe based on C=N isomerization for the selective detection of formaldehyde in living cells and *in vivo*†

Xinyu Song,[a,b] Xiaoyue Han,[b,d] Fabiao Yu, *[b,c] Jinjin Zhang,[a,c] Lingxin Chen *[b,c] and Changjun Lv*[a,c]

Formaldehyde (FA) is an endogenously produced reactive carbonyl species (RCS) through biological metabolic processes whose concentration is closely related to human health and disease. Noninvasive and real-time detection of FA concentration in organisms is very important for revealing the physiological and pathological functions of FA. Herein, we design and synthesize a reversible fluorescent probe BOD-NH_2 for the detection of FA in living cells and *in vivo*. The probe is composed of two moieties: the BODIPY fluorophore and the primary amino group response unit. The probe undergoes an intracellular aldimine condensation reaction with FA and forms imine (C=N) which will result in C=N isomerization and rotation to turn-off the fluorescence of the probe. It is important that the probe can show a reversible response to FA. The probe BOD-NH_2 has been successfully applied for detecting and imaging FA in the cytoplasm of living cells. BOD-NH_2 is capable of detecting fluctuations in the levels of endogenous and exogenous FA in different types of living cells. The probe can be used to visualize the FA concentration in fresh hippocampus and the probe can further qualitatively evaluate the FA concentrations in *ex vivo*-dissected organs. Moreover, BOD-NH_2 can also be used for imaging in mice. The above applications make our new probe a potential chemical tool for the study of physiological and pathological functions of FA in cells and *in vivo*.

Received 8th September 2017,
Accepted 30th November 2017

DOI: 10.1039/c7an01488k

rsc.li/analyst

Introduction

Formaldehyde (FA) has long been recognized as an environmental pollutant and toxin which is commonly released from plywood manufacturing and vehicle exhaust.[1] The toxicity of FA has been utilized in applications as a tissue fixative and an embalming agent.[2] However, FA is now considered to be a primary type of endogenous reactive carbonyl species (RCS) produced in biological processes ranging from epigenetics to one carbon metabolism.[3] The strong electrophilicity of FA enables its reactivity with a variety of biological nucleophiles, which can be beneficial or pernicious to physiological functions depending on the circumstances. FA can be endogenously generated in biological systems during metabolic processes, including mitochondrial one-carbon metabolism, nuclear epigenetic modifications, and metabolite oxidation by demethylase and oxidase enzymes such as lysine specific demethylase 1 (LSD1) and JmjC domain-containing proteins, as well as semicarbazide-sensitive amine oxidase.[4] Intracellular FA is preserved at relatively higher concentration under normal physiological conditions, reaching up to a steady state level of 200–500 μM in certain cells and 50–100 μM in blood.[5] In brain, the level of FA has been determined to be in the range of 200–400 μM, which implies the important role of FA in the storage, preservation, and retrieval of long-term memory.[6] Therefore, the maintenance of FA concentration homeostasis in cells is critical and necessary for cell signaling. A high concentration of FA (>800 mM) is associated with an increased risk of a variety of diseases, such as neurodegenerative diseases, cancer, diabetes, chronic liver and heart disorders and asthma.[7] Although the International Agency for Research on Cancer (IARC) has classified FA as a human carcinogen, which is associated with cancer such as nasopharyngeal carcinoma and sinus cancer, FA certainly acts as a key signaling molecule in the course of disease development. Moreover, FA may also be a target for drug release. Therefore,

[a]*Department of Respiratory Medicine, Binzhou Medical University Hospital, Binzhou 256603, China. E-mail: lucky_lcj@sina.com*
[b]*Key Laboratory of Coastal Environmental Processes and Ecological Remediation, Yantai Institute of Coastal Zone Research, Chinese Academy of Sciences, Yantai 264003, China. E-mail: fbyu@yic.ac.cn, lxchen@yic.ac.cn*
[c]*Medicine Research Center, Institute of Molecular Medicine, Binzhou Medical University, Yantai 264003, China*
[d]*University of Chinese Academy of Sciences, Beijing 100049, China*
†Electronic supplementary information (ESI) available: Additional information on experiments. See DOI: 10.1039/c7an01488k

FA-related molecular mechanisms are important for disease prediction and therapy. As a member of endogenous RCS, the intracellular concentration of FA is always changing. The ability to accurately detect the changes in the levels of FA is important for the study and treatment of the disease.

Several methods have been designed for the sensitive detection of FA, involving radiometry, colorimetric assays,[8] gas chromatography (GC),[9] mass spectrometry (MS)[10] and high-performance liquid chromatography (HPLC).[11] But most of them fail to meet the requirement of *in situ* and real-time non-destructive detection. As is known, intracellular FA concentration homeostasis is a complex dynamic process in living systems. The process includes signal transduction, homeostasis regulation, and rapid elimination in time in certain organelles. New biological detection technologies that allow dynamic detection of FA fluctuations in living systems can help interpret the physiological and pathological dichotomy of this simple RCS.

Compared with other biological detection technologies, fluorescence bioimaging technology has become a powerful supporting tool for investigating physiological and pathological processes of interest because of its many advantages, such as good sensitivity, excellent selectivity, rapid response, and non-invasive detection.[12] In particular, fluorescent probes based on small artificial organic molecules can offer rational regulation mechanisms for determining various detection parameters at the biomolecular level with high spatial and temporal resolution. Small molecule fluorescent probes have been successfully employed to detect a variety of biological analytes, such as reactive oxygen species, reactive nitrogen species, reactive sulfur species, ions and anions, as well as changes in pH.[13] Fluorescent probes have emerged as a promising chemical tool for the detection of FA with high selectivity and sensitivity in living systems.[14] The currently available fluorescent probes for detection of FA include 2-aza-Cope reaction-based detection,[15] formimine-based detection,[16] and aminal-based detection.[17] However, intracellular FA homeostasis is a complex process in living systems. Most of the previously reported probes are irreversible ones for the detection of FA. Until now, there were few reversible probes for indicating the dynamic homeostasis of endogenous FA.[16e] In this regard, developing a probe that can respond reversibly to the changes in FA *via* a reactive-based mechanism for visualizing the states of this homeostasis cycles remains an urgent requirement.[18]

Herein, we proposed a reversible fluorescent probe BOD-NH_2 for the selective and sensitive detection of FA to examine the pathophysiological roles of FA more accurately. The probe was composed of two moieties: a fluorophore BODIPY and a response unit primary amino group. BOD-NH_2 underwent an aldimine condensation reaction with FA. The fluorescence signal change mechanism was attributed to C=N isomerization (Scheme 1). The probe could selectively and sensitively detect FA in a reversible manner with a low limit of detection at 50 nM ($3\sigma/\kappa$) under the experimental conditions. The endogenous and exogenous FA concentration changes were successfully detected by BOD-NH_2. Our results demonstrated that the different levels of FA depend on different cell lines. The overall levels of FA have a close relationship with the enzyme LSD1. Furthermore, assays with imaging of FA in the hippocampus and in mice highlighted the potential application of BOD-NH_2 for the physiological roles of FA *in vivo*.

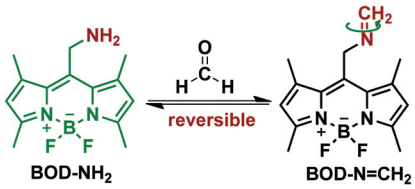

Scheme 1 The structure of BOD-NH_2 and the proposed reaction mechanism for FA detection.

Results and discussion

Design and reversible mechanism of BOD-NH_2

We attempted to construct a selective and sensitive fluorescent probe BOD-NH_2 for the intracellular FA detection. We chose a BODIPY fluorophore as the fluorescence signal transduction moiety due to its high fluorescence quantum yield, good light stability, excellent molar extinction coefficient and favorable pH stability.[19] A primary amino group was selected as the response unit (Scheme 1). Contrary to the expected, the primary amino group did not regulate the photoinduced electron transfer process (PET) towards the BODIPY fluorophore.[13a,20] After the probe reacted with FA *via* an aldimine condensation reaction, it would yield an imine (C=N) group. The C=N isomerization and rotation could lead to an energy decay phenomenon in the excited state of the BODIPY fluorophore, and then resulted in energy loss, which quenched the fluorescence emission of the probe.[21] To verify the proposed fluorescence quenching mechanism, we investigated the fluorescence response of the imine BOD-NH=CH_2 towards viscosity.[21] As the viscosity of the solution increased, the isomerization and rotation were restrained, and the fluorescence recovered (Fig. S8†). Moreover, the newly formed imine BOD-NH=CH_2 could be easily hydrolyzed in aqueous solution. This response mechanism made the reversible detection of FA possible. The synthesis of BOD-NH_2 is illustrated in Scheme 2.

Spectral properties of BOD-NH_2

The absorption and fluorescence spectra of BOD-NH_2 (10 μM) were examined under simulated physiological conditions

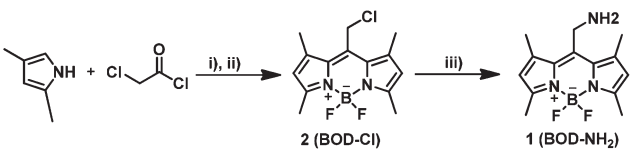

Scheme 2 The synthesis routes of BOD-NH_2. (i) CH_2Cl_2, reflux, 10 h. (ii) NEt_3, $BF_3{\cdot}OEt_2$, 76%. (iii) THF, $NH_3{\cdot}H_2O$, 25 °C, 1 h; THF, 4 h, 82%.

(10 mM HEPES buffer, pH 7.4). As shown in Fig. 1a, the maximum absorption wavelength of BOD-NH_2 was 495 nm ($\varepsilon_{495\ nm}$ = 1.969 × 10^4 M^{-1} cm^{-1}, Φ = 0.85). After the addition of FA, the absorption spectra of the probe have no significant change. The fluorescence titration of BOD-NH_2 was performed in the presence of FA with a concentration ranging from 0 to 500 μM. The fluorescence quantum yield reduced to Φ = 0.01. As shown in Fig. 1b, the corresponding fluorescence emission profiles decreased with peaks centered at 515 nm. There was a linear concentration-dependent fluorescent response with BOD-NH_2 towards FA ranging from 0 to 500 μM (Fig. 1c), and the calibration curve was $F_{515\ nm}$ = −2.09 × 10^4 [FA] μM + 1.06 × 10^3 with a linear fitting constant r = 0.9991. The results revealed that our probe could be used to detect FA qualitatively and quantitatively. The limit of detection was calculated as 50 nM ($3\sigma/k$) under the experimental conditions indicating the high sensitivity of our probe BOD-NH_2 towards the detection of FA.

Kinetics and reversible response towards FA

Next, the reaction kinetics of BOD-NH_2 (10 μM) towards FA (500 μM) was evaluated under simulated physiological conditions (10 mM HEPES buffer, pH 7.4). As shown in Fig. 1c, FA (500 μM) was added at 10 min. The fluorescence intensity decreased to platform within 2 h. The results demonstrated that the probe BOD-NH_2 could be employed to detect the changes of FA in living cells and *in vivo*. We next verified whether our probe could reversibly monitor FA change cycles in solution. As illustrated in Fig. 1c, the probe was first treated with FA (500 μM) for 2 h with the fluorescence switch-off. After maintaining the platform for more than 1 h, sodium bisulfite ($NaHSO_3$, 500 μM) was added as a scavenger to eliminate FA. As expected, the fluorescence emission could rapidly recover and reach almost the original fluorescence intensity in 10 min in HEPES buffer. The reversible cycle could be repeated at least

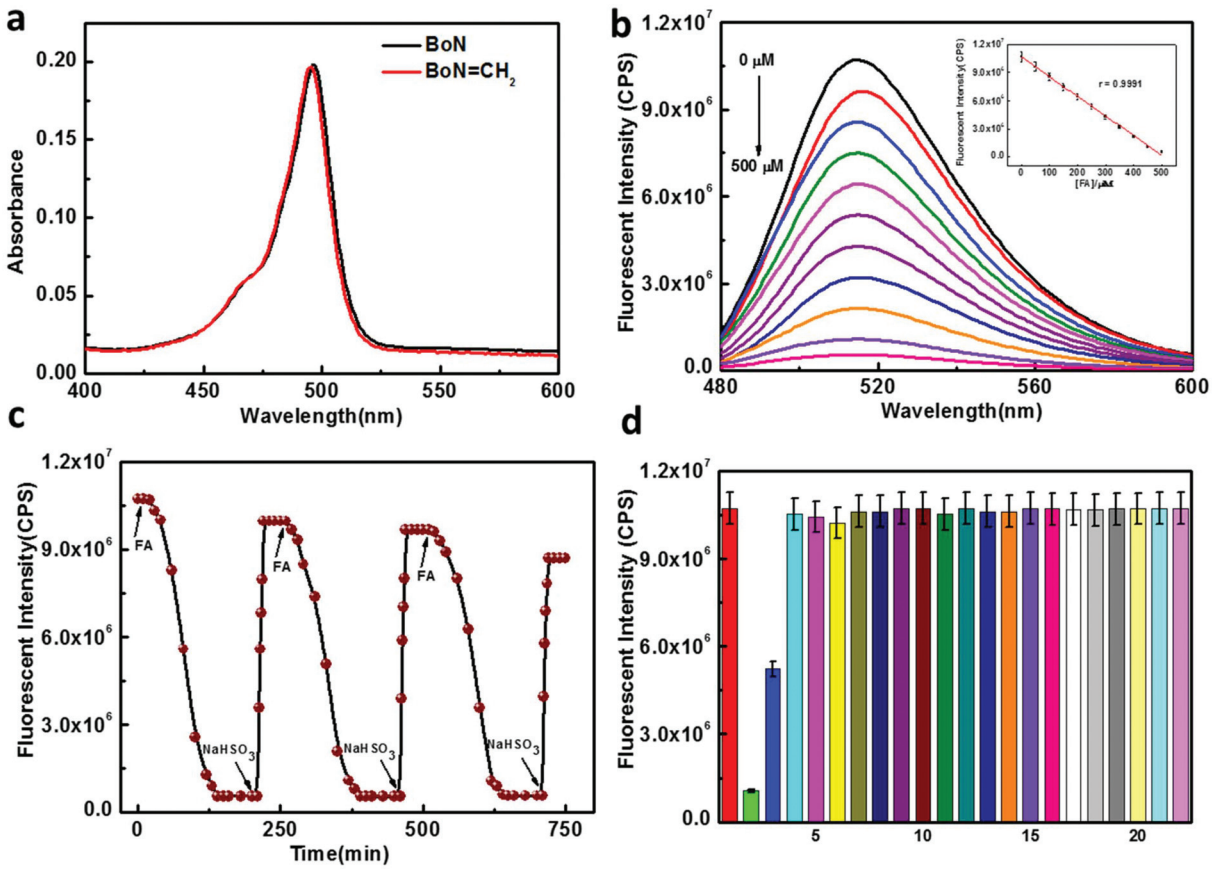

Fig. 1 (a) Absorption spectra of probe BOD-NH_2 (10 μM) before and after addition of 500 μM FA. (b) Fluorescence spectra of BOD-NH_2 (10 μM) upon addition of FA (0–500 μM). Inset: The linear relationship between the fluorescence intensity at 515 nm and FA concentrations in HEPES (10 mM, pH 7.4) at 37 °C. (c) Time-dependent response cycles of BOD-NH_2 (5 μM) towards FA. FA was added at the reaction of 10 min in 10 mM HEPES buffer (pH 7.4, 0.5% Tw 80). 2 h later, the solution was treated with 500 μM $NaHSO_3$. When fluorescence returned to the starting levels, another 1 equiv. of FA was added to the mixture. The redox cycle was repeated 3 times. (d) Fluorescence responses of BOD-NH_2 (5 μM) to bio-relevant RCS, amino acids, and other relevant biological species. The bars represented relative responses at 515 nm of BOD-NH_2 to the analytes: 1, blank; 2, FA (500 μM); 3, FA (500 μM) then 250 μM $NaHSO_3$; 4, FA (500 μM) then 500 μM $NaHSO_3$; 5, acetaldehyde (50 μM); 6, methylglyoxal (50 μM); 7, glyoxal (50 μM); 8, benzaldehyde (50 μM); 9, pyridoxal (50 μM); 10, 4-nitro-benzaldehyde (50 μM); 11, sodium pyruvate (5 mM); 12, alanine (400 μM); 13, glycine (5 mM); 14, serine (5 mM); 15, arginine (5 mM); 16, cysteine (5 mM); 17, glutathione (5 mM); 18, glucose (1 mM); 19, hydrogen peroxide (100 μM); 20, hydrogen sulfide (100 μM); 21, methane acid (100 μM); and 22, dehydroascorbate (100 μM). All the above data were recorded in 10 mM HEPES buffer (10 mM, pH 7.4) at 37 °C for 2 h. λ_{ex} = 495 nm, λ_{em} = 515 nm. The data are shown as mean (±s.d.) (n = 7).

3 times with only a little fluorescence decrement (>5% fluorescence intensity of BOD-NH_2 was bleached during the process). The spectral profile changes are shown in Fig. S1.† The result displayed that BOD-NH_2 was suitable for reversible detection in living cells.

Selectivity

Standard fluorescence pH titrations were performed in 10 mM HEPES solution at a concentration of 10 μM BOD-NH_2. As shown in Fig. S2,† the pH values of the media hardly have effects on the fluorescence intensity within a range from 4.0 to 9.2.[13a] We suggested that the probe BOD-NH_2 would work well under physiological conditions (pH = 7.4). We next evaluated the selectivity of BOD-NH_2 towards FA upon addition of various typical bio-relevant RCS, other bio-relevant biological species, as well as anions and cations. The fluorescence responses to the bio-relevant species were obtained at the time points of 2 h. As shown in Fig. 1d and Fig. S6,† only FA could switch the strong fluorescence emission off. Other RCS including acetaldehyde, methylglyoxal, glyoxal, benzaldehyde, pyridoxal, and 4-nitrobenzaldehyde could not induce any fluorescence intensity changes. Additionally, the fluorescence intensity of BOD-NH_2 was also hardly affected by other relevant biological species, such as sodium pyruvate, alanine, glycine, serine, arginine, cysteine, glutathione, glucose, hydrogen peroxide, hydrogen sulfide, methane acid and dehydroascorbate. And the addition of different concentrations of $NaHSO_3$ (250 and 500 μM) would turn on the fluorescence emission to a different extent (Fig. 1d). All the results demonstrated that BOD-NH_2 was highly selective for FA over other RCS, and other relevant biological species. Clearly, our probe BOD-NH_2 could potentially meet the requirement for the detection of FA in complex biological samples.

Cytotoxicity and imaging of exogenous FA level changes

After being confirmed to be a selective chemical tool for FA detection in aqueous buffer, the probe BOD-NH_2 was applied to assess its capability for detecting exogenous FA level changes in living cells. Prior to cell tests, a MTT experiment was performed to evaluate the cytotoxicity of BOD-NH_2. SMMC-7721, HEK, and PC9 cells were incubated with 0–80 μM probe for 24 h, and then the cytotoxicity was measured (Fig. S3†). The result of cell viability indicated that 5 μM BOD-NH_2 displayed low cytotoxicity to living cells under experimental conditions. Cell imaging experiments were performed by utilizing a laser scanning confocal microscope. SMMC-7721 cells were treated with 0–200 μM FA for 60 min, washed three times with fresh DMEM (Dulbecco's modified Eagle's medium), and then incubated with 5 μM BOD-NH_2 for another 60 min at 37 °C in DMEM. Finally the excess probe was removed by washing with fresh DMEM three times. As shown in Fig. 2a and c, the addition of FA decreased the fluorescence intensity in cells. The result demonstrated that the addition of FA was captured by our probe. Flow cytometry analysis which allows rapid analysis of millions of cells and generates statistically convincing data can be applied to verify the results obtained from laser scanning confocal microscope imaging.

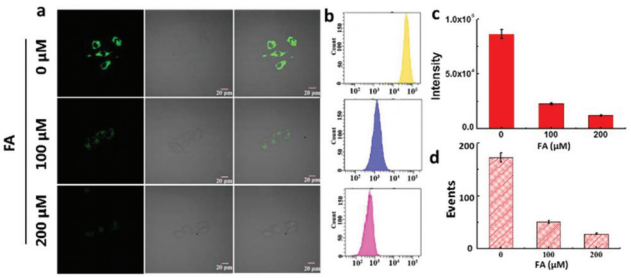

Fig. 2 Fluorescence imaging of exogenous FA level changes in living SMMC-7721 cells. Images show fluorescence intensities collected in an emission window from 500 to 550 nm, and the excitation wavelength was set at 488 nm. (a) SMMC-7721 cells were first treated with 0, 100 and 200 μM FA for 1 h, and then the cells were incubated with 5 μM BOD-NH_2 for 60 min, respectively. (b) Flow cytometry analysis of (a). (c) Mean fluorescence intensities of (a). (d) Mean values of (b). The data are shown as mean (±s.d.) (n = 7).

Next, flow cytometry experiments were performed to confirm the above results. The results in Fig. 2b and d were consistent with the results of confocal microscopy imaging shown in Fig. 2a and c. These results indicated that our probe could be used to image exogenous FA level changes in living cells.

Imaging of endogenous FA concentration fluctuations

Encouraged by the successful application of BOD-NH_2 in imaging exogenous FA level changes, the metabolism induced endogenous FA concentration fluctuations in living cells were further analyzed using our probe. LSD1 is a flavin-dependent histone demethylase that demethylates mono- and di-methylated lysines to release FA. Tranylcypromine (TCP, IC_{50}: 2 μM) and *N*-((1*R*,2*S*)-2-phenylcyclopropyl)piperidin-4-amine (GSK-LSD1, IC_{50}: 42 nM) can irreversibly inhibit the expression of LSD1.[15b] To validate whether BOD-NH_2 could detect endogenous FA in living cells, we incubated SMMC-7721 cells with BOD-NH_2 for 60 min. The cells exhibited a relatively low fluorescence signal indicating a low level of FA in SMMC-7721 cells (Fig. 3a and c). The cells in the 2nd group were pre-incubated with TCP (20 μM) for 20 h. These cells showed a higher fluorescence intensity (Fig. 3a and c). The result demonstrated that our probe could detect a FA level decrease which was induced by TCP. Furthermore, the cells in the third group were pretreated with 12 μM GSK-LSD1 for 20 h. Much stronger fluorescence was obtained as shown in Fig. 3a and c, which indicated a lower FA concentration in cells. The results of flow cytometry analysis were consistent with the results obtained from confocal fluorescence images (Fig. 3b and d). In order to verify that the decrease of FA concentration resulted from the inhibition expression of the LSD1 enzyme, we conducted western blot analysis to examine the expression of the LSD1 protein. The expression of LSD1 was inhibited by TCP to a moderate degree, but severely suppressed by GSK-LSD1 to a large extent. The LSD1 expression was consistent with the FA level change which was detected by our probe BOD-NH_2. The result revealed that our probe could be utilized to image the endogenous FA concentration fluctuations in living cells.

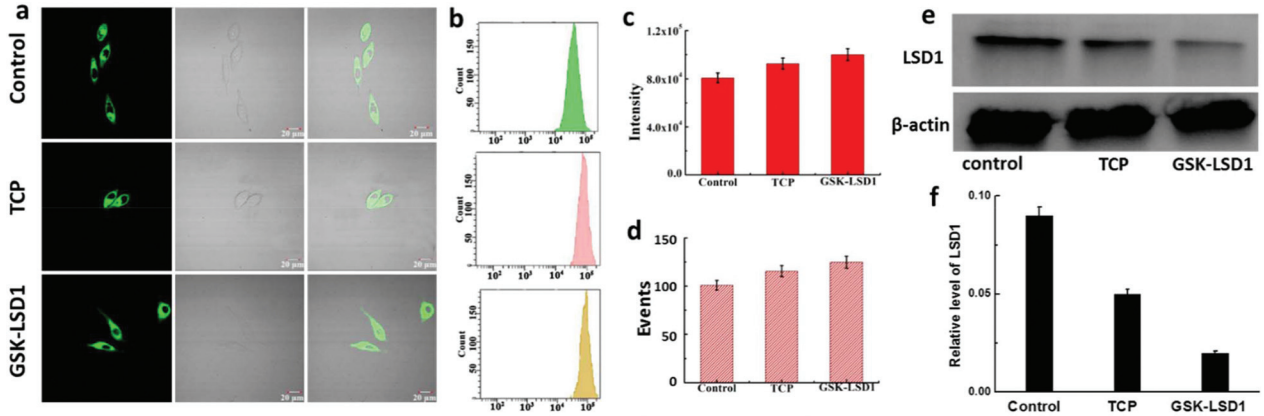

Fig. 3 Fluorescence imaging of endogenous FA concentration fluctuations in living SMMC-7721 cells. Images show fluorescence intensities collected in an emission window from 500 to 550 nm, and excited at 488 nm. (a) SMMC-7721 cells were treated with TCP (20 μM) for 20 h and GSK-LSD1 (12 μM) for 20 h. Then the cells were incubated with probe BOD-NH_2 (5 μM) for 60 min; before imaging the cells were washed three times with fresh DMEM. (b) Flow cytometry analysis of (a). (c) Mean fluorescence intensities of (a). (d) Mean fluorescence intensities of (b). (e) Western blotting analysis of LSD1 expression shown in (a). (f) Histograms of protein expression shown in (e). The data are shown as mean (±s.d.) (n = 7).

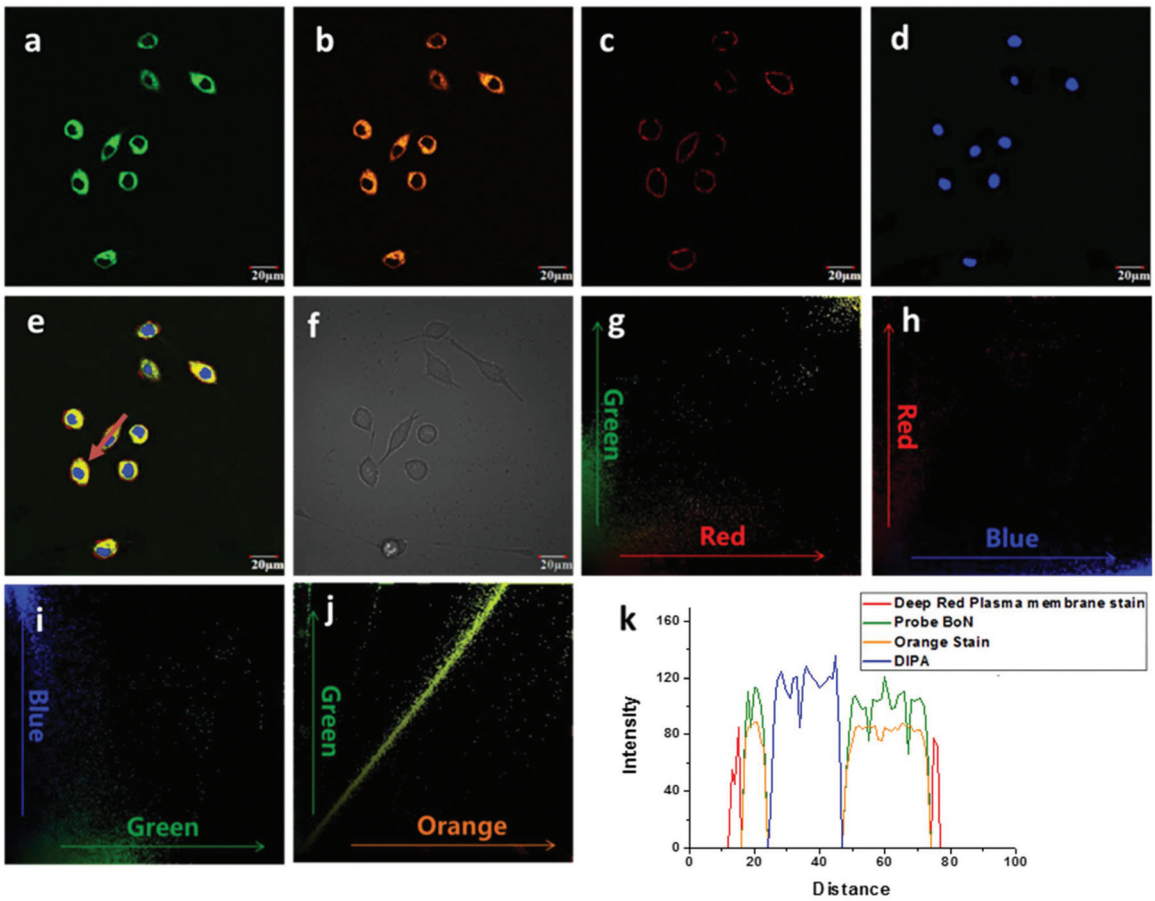

Fig. 4 Sublocation images of BOD-NH_2 (5 μM), Calcein-AM (1 μg mL^{-1}), Deep Red plasma membrane stain (1 μg mL^{-1}), and DAPI (1 μg mL^{-1}) in living SMMC-7721 cells. SMMC-7721 cells were pretreated with GSK-LSD1 (2 μM) for 20 h, and then washed three times with DMEM. The cells were then costained with DAPI for 30 min, Orange stain and Deep Red plasma membrane stain for 15 min, and with BOD-NH_2 for 15 min. The images were acquired using BOD-NH_2 with (a) Orange stain, (b) Deep Red plasma membrane stain and (c) DAPI. (d) Fluorescence images were acquired in the fluorescence collection windows from 500 to 550 nm for (a), from 550 to 600 nm for (b), from 650 to 700 nm for (c), from 425 to 500 nm for (d), λ_{ex} = 495 nm, 535 nm, 635 nm and 405 nm, respectively. (e) Overlay image of (a), (b) and (c). (f) Bright-field image of (a). (g) Pixel correlation plot between the green and red channels. (h) Pixel correlation plot between the red and blue channels. (i) Pixel correlation plot between the blue and green channels. (j) Pixel correlation plot between the green and orange channels. (k) Intensity profiles of regions of interest (red arrow in e) across SMMC-7721.

Sublocation in cells

It has been demonstrated that the probe BOD-NH_2 could detect the exogenous and endogenous FA level changes in cells, and we further performed colocalization experiments to examine the intracellular location of BOD-NH_2. We introduced a cytoplasm targetable dye Calcein-AM (Fig. 4b), a cell membrane localization dye Deep Red plasma membrane stain (Fig. 4c) and a nucleus fluorescence marker DAPI (Fig. 4d) to confirm the intracellular location of BOD-NH_2 in SMMC-7721 cells. The SMMC-7721 cells were pretreated with GSK-LSD1 (2 μM) for 20 h and then imaged using BOD-NH_2 (Fig. 4a). As shown in Fig. 4e, the fluorescence images of BOD-NH_2 show a consistent overlap with Calcein-AM in the cytoplasm, while the probe hardly showed any overlap with the nucleus dye DAPI and cell membrane localization dye Deep Red plasma membrane stain (Fig. 4). We also analyzed the pixel correlation between the color-pair intensity shown in Fig. 4e. The results are shown in Fig. 4g–j. Only the distribution of BOD-NH_2 and Calcein-AM exhibited a highly correlated plot. The Pearson's colocalization coefficient between BOD-NH_2 and Calcein-AM was determined to be R_r = 0.99, and the Manders' coefficients were m_1 = 0.98 and m_2 = 0.97. The results illustrated that BOD-NH_2 could locate in the cytoplasm to detect FA dynamic changes in cells.

Imaging of intracellular FA in different cell lines

In order to confirm the general utilization of our probe to detect FA in cells, BOD-NH_2 was applied to a variety of cell lines for imaging the levels of FA. Seven types of cell lines were selected to conduct our tests: SMMC-7721, HEK, PC9, HeLa, HepG2, SH-SY5Y and A549. All the cell lines were incubated with 5 μM BOD-NH_2 at 37 °C for 60 min, and then washed with DMEM three times before imaging. As shown in Fig. 5a (control), the fluorescence intensity varied with different FA levels in the seven types of cell lines. Then 200 μM FA was added to the above cells over 60 min. The fluorescence intensity in the seven cell lines decreased (Fig. 5a, FA). The result indicated that the addition of FA was also captured by our probe. The average fluorescence intensity shown in Fig. 5a demonstrated that different cell lines might provide different carrying capacities for FA (Fig. 5b). The above results were

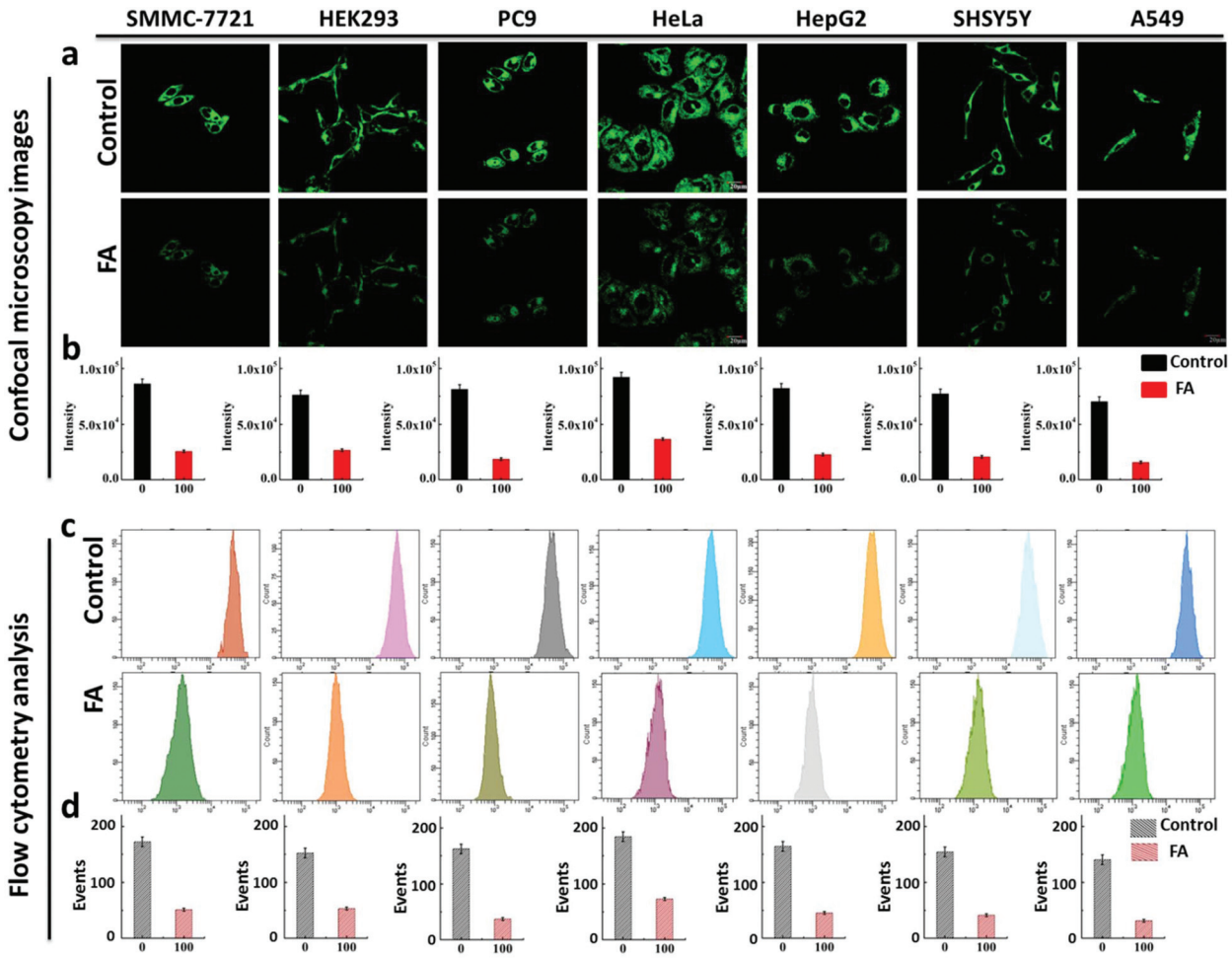

Fig. 5 (a) Fluorescence imaging of exogenous and endogenous FA in SMMC-7721 cells, HEK293 cells, PC9 cells, HeLa cells, HepG2 cells, SHSY5Y cells and A549 cells using BOD-NH_2 FA. (b) Mean fluorescence intensities of (a). (c) Flow cytometry analysis of (a). (d) Mean fluorescence intensities of (c). The data are shown as mean (±s.d.) (n = 7).

further verified by flow cytometry analysis. The results shown in Fig. 5c and d were consistent with the confocal microscopy image results shown in Fig. 5a and b. All the results revealed that BOD-NH_2 could respond to the intracellular FA level changes in different cell lines.

Reversible response towards FA in living cells

We next applied the probe BOD-NH_2 to verify the possibility of reversible fluorescence imaging of FA in living cells. As shown in Fig. 6a, after the HepG2 cells were incubated with 5 μM BOD-NH_2 for 1 h, strong fluorescence emission was observed. After the addition of 100 μM FA for 1 h, the fluorescence signal decreased. When $NaHSO_3$ (100 μM) was added over 10 min to absorb FA in cells, the fluorescence recovered. The addition of another dose of FA resulted in reduced fluorescence. These cycles were successfully repeated three times (Fig. 6b), which indicated the reversible ability of the probe in living cells. Moreover, flow cytometry analysis was conducted to further verify the above results. As shown in Fig. 6c and d, the flow cytometry analysis results were consistent with the confocal microscopy image results (Fig. 6a and b). All the results demonstrated that probe BOD-NH_2 could be used for reversible detection of FA in living cells.

Evaluation of FA levels in organs

The probe has been successfully used for the reversible detection of FA in living cells; we next applied the probe for the qualitative analysis of FA levels in *ex vivo*-dissected organs. The organs were treated as tissue homogenates (1 g tissue in 10 mL of saline). After centrifugation, the supernatant was used for our tests. The results shown in Fig. 7 showed that different organs contain different concentrations of FA. The levels of FA in the liver and heart were much higher than other organs, such as spleen, kidneys, lungs and brain (hippocampus and cortex). The reason might be attributed to the higher expression of the LSD1 enzyme in the liver and heart.[22] Our tests were basically consistent with the reported data.[15–17,23] The results indicated that the probe BOD-NH_2 could be applied to qualitatively evaluate FA concentrations in *ex vivo*-dissected organs.

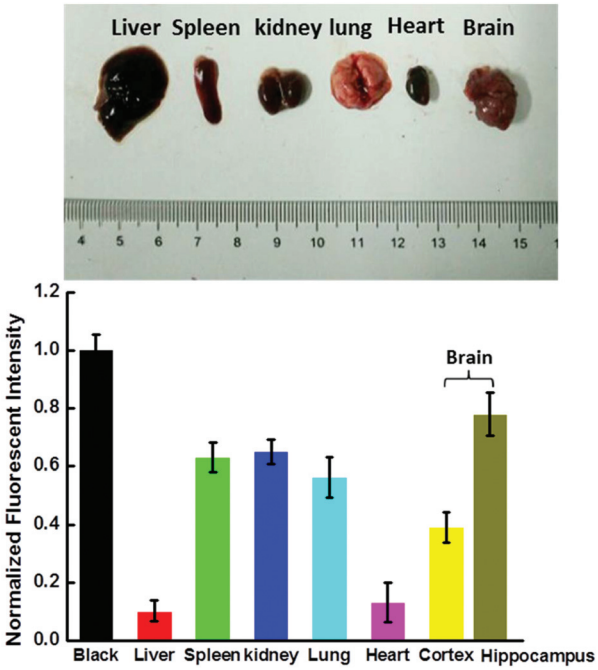

Fig. 7 Qualitative evaluations of FA concentrations in *ex vivo*-dissected organs. Black: the fluorescence response to 10 μM FA in 10 mM HEPES buffer with 15% serum for 1 h at 37 °C. Other bars: fluorescence responses to *ex vivo*-dissected organs: liver, spleen, kidneys, lungs, heart, and brain (hippocampus and cortex). The normalized fluorescence intensities are presented. λ_{ex} = 495 nm, λ_{em} = 515 nm. The data are shown as mean (±s.d.) (n = 7).

Bioimaging FA in mouse hippocampus

The hippocampus of the brain is mainly responsible for memory and learning, which is closely related to brain health.[24] FA can take part in the DNA demethylation cycle for long-term memory storage, preservation and recovery role in the brain. In a healthy person, the FA concentration in the brain is about 0.2 mM (hippocampus) and 0.4 mM (cortex).[23] To explore the relationship between FA concentration fluctuations and brain disease, the detection of FA in the hippocampus of the brain was pretty important. The fresh hippo-

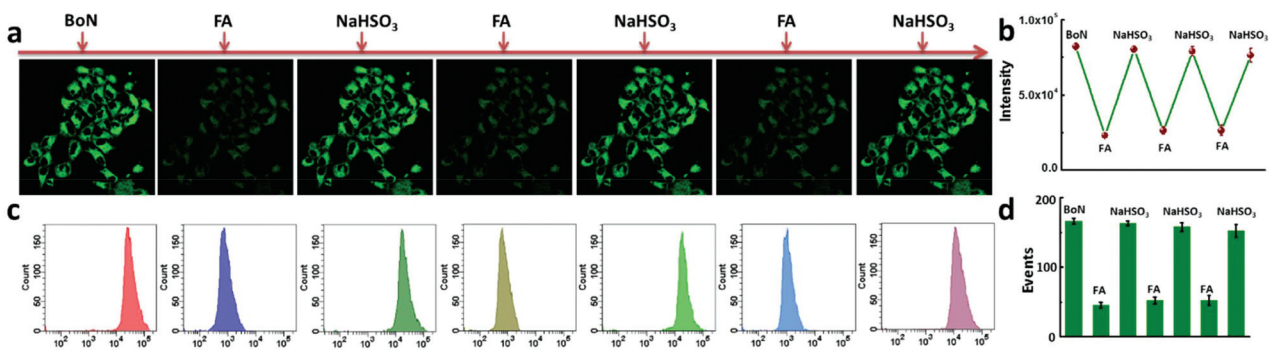

Fig. 6 (a) Reversible fluorescence imaging of BOD-NH_2 (5 μM) after the sequential treatment of FA (100 μM, 1 h) and $NaHSO_3$ (100 μM, 10 min) in HepG2 cells. (b) Mean fluorescence intensities of the cycles in (a). (c) Flow cytometry analysis of (a). (d) Mean fluorescence intensities of (c). The data are shown as mean (±s.d.) (n = 7).

campal tissue sections were obtained from 4–6 week old mice. Before imaging, the slices were incubated with DAPI for 30 minutes and then incubated with the probe BOD-NH_2 for 60 min. As shown in Fig. 8a, the structure of the hippocampus is well imaged using BOD-NH_2. After addition of $NaHSO_3$, the fluorescence of the hippocampus slice increased (Fig. 8d), which indicated the decrease of FA concentration.[16b] The images of the nucleus stained by DAPI are shown in Fig. 8b and e. Fig. 8c shows the overlay images of Fig. 8a and b. Fig. 8f shows the overlay images of Fig. 8d and e. To verify the tissue imaging ability of our probe, we imaged 20–120 μm deep axial planes with 10 μm as interval to reconstruct three-dimensional (3D) images. The 3D images of Fig. 8a–c along the *z*-direction with depths of 20–120 μm are illustrated in Fig. 8g–i. The *Z*-stack image for hippocampus showed activation of the fluorescence signal even at a depth of 100 μm, indicating that the fluorescence signal of probe BOD-NH_2 could penetrate the hippocampus slice with a thickness of 100 μm (Fig. 8j). All the

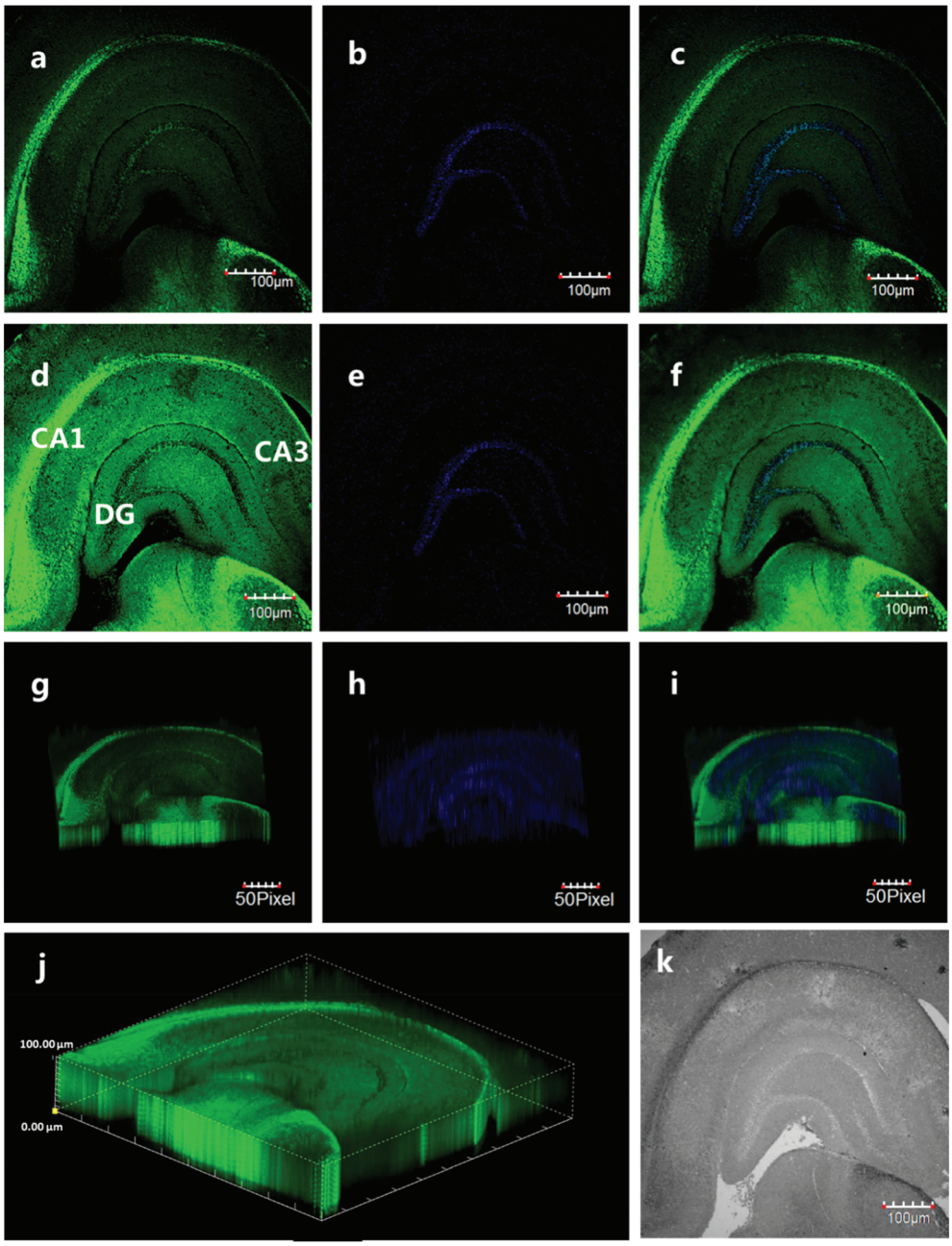

Fig. 8 Fluorescence imaging of slices of fresh mouse hippocampus. (a) Fluorescence imaging of hippocampus with probe BOD-NH_2 (10 μM). (b) Fluorescence imaging with DAPI (5 μg mL^{-1}). (c) Overlay image of (a) and (b). (d) Fluorescence imaging of slices of fresh hippocampus with $NaHSO_3$ (50 μM). (e) Fluorescence imaging of DAPI after addition of $NaHSO_3$. (f) Overlay image of (d) and (e). (g) 3D image of (a). (h) 3D image of (b). (i) 3D image of (c). (j) Perspective for 3D image of (d). (k) Bright-field image of fresh mouse hippocampus. BOD-NH_2 and DAPI images show fluorescence intensities collected in the emission windows from 500 nm to 550 nm and 425 nm to 500 nm, excitation at 488 nm and 405 nm, respectively.

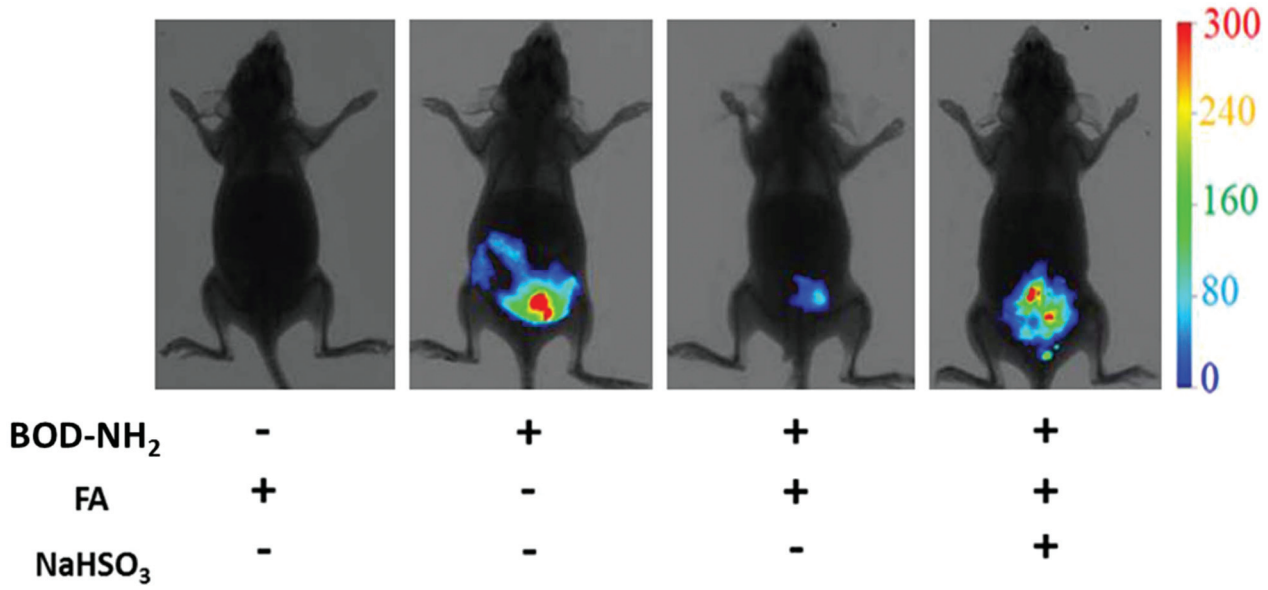

Fig. 9 Fluorescence image of FA level changes in the peritoneal cavity of BALB/c mice. (a) Group a was injected in the i.p. cavity with FA (500 μM, 50 μL in 1 : 9 DMSO/saline, v/v) for 1 h as the control. (b) Group b was injected in the i.p. cavity with BOD-NH_2 (50 μM, 50 μL in 1 : 9 DMSO/saline, v/v) for 1 h. (c) Group c was injected in the i.p. cavity with FA (500 μM, 50 μL in 1 : 9 DMSO/saline, v/v) for 1 h and then injected i.p. with BOD-NH_2 (50 μM, 50 μL in 1 : 9 DMSO/saline, v/v) for another 1 h. (d) Group d was pretreated as described in group c, but given $NaHSO_3$ (500 μM, 100 μL in 1 : 9 DMSO/saline, v/v) for one more hour.

results indicated that our probe could be applied to bioimaging of FA in mouse hippocampus and was capable of detecting FA in tissues.

Bioimaging FA *in vivo*

We next examined the possibility of BOD-NH_2 for imaging FA *in vivo* using an *In vivo* Imaging System. BALB/c mice were divided into four groups (Fig. 9). The mice in group a were given an intraperitoneal (i.p.) injection of FA (500 μM, 50 μL in 1 : 9 DMSO/saline, v/v) for 1 h as the control (Fig. 9a). The mice in group b were given an intraperitoneal (i.p.) injection of BOD-NH_2 (50 μM, 50 μL in 1 : 9 DMSO/saline, v/v) for 1 h. The strong fluorescence signal shown in Fig. 9b demonstrated that our probe could be used for imaging *in vivo*. The mice in group c were injected in the i.p. cavity with FA (500 μM, 50 μL in 1 : 9 DMSO/saline, v/v) for 1 h and then injected i.p. with BOD-NH_2 (50 μM, 50 μL in 1 : 9 DMSO/saline, v/v) for another 1 h. The slight fluorescence signal indicated the detection of FA levels in the abdominal cavity of mice. The mice in group d were pretreated as described in group c, but given $NaHSO_3$ (500 μM, 100 μL in 1 : 9 DMSO/saline, v/v) for one more hour. The fluorescence intensity of group d was higher than that of group c, which resulted from the depletion of FA by $NaHSO_3$ *in vivo*. The results revealed that the probe was capable of bioimaging FA level changes *in vivo*.

Conclusions

In conclusion, we have designed and synthesized a reversible fluorescent probe for the selective detection of FA in living cells and *in vivo*. The probe employed a BODIPY fluorophore as the fluorescence signal transducer and a primary amino group as the fluorescence modulator. The probe is capable of reversible detection of FA without interference from other RCS and bio-relevant species. BOD-NH_2 can localize in the cytoplasm and track the exogenous and endogenous FA concentration fluctuations in cells. The probe also demonstrates that different cell lines possess various FA levels. Moreover, BOD-NH_2 is successfully applied to detect FA concentrations in *ex vivo*-dissected organs. The bioimaging assays in hippocampus and peritoneal cavity of BALB/c mice illustrate the application of our probe in deep tissue. We hope the probe can contribute to the study of FA associated with normal and pathological processes.

Experimental section

Synthesis and characterization of probe BOD-NH_2

Synthesis of BOD-Cl. 2,4-Dimethylpyrrole (0.4 mL, 3.89 mmol) was dissolved in 10 mL anhydrous CH_2Cl_2 under an Ar atmosphere. Chloroacetyl chloride (0.15 mL, 1.95 mmol) was added dropwise, and then refluxed for 10 h. The reaction was traced by thin layer chromatography. After the reaction was complete, distilled trimethylamine (NEt_3, 4 mL, 28.65 mmol) and boron trifluoride etherate ($BF_3{\cdot}OEt_2$, 8 mL, 7.52 mmol) were added dropwise into the above solution. The solvent was removed using a rotary evaporator and the remaining residue was purified through silica gel chromatography (200–300 mesh) eluted with petroleum ether : ethyl acetate =

6 : 1 (v/v). Compound **2** was afforded as a red solid (0.437 g, yield: 76%). ^{1}H NMR ($CDCl_3$-D^1, 500 MHz) δ (ppm): 6.10 (s, 2H), 4.79 (s, 2H), 2.46 (s, 12H). ^{13}C NMR ($CDCl_3$-D^1, 125 MHz) δ (ppm): 156.72, 141.23, 136.02, 131.30, 122.26, 37.10, 15.47, 14.62. LC-MS (ESI$^+$): *m*/*z* $C_{14}H_{16}BClF_2N_2$ calcd 296.5513, found [M] 296.5512.

Synthesis of BOD-NH$_2$. Tetrahydrofuran (THF, 40 mL) and ammonia ($NH_3{\cdot}H_2O$, 80 mL, 29.3%) were stirred in a 250 mL round bottom flask at 25 °C for 1 h. BOD-Cl (1.48 g, 3.89 mmol) was dissolved in 80 mL THF and added dropwise into the round bottom flask using a constant pressure dropping funnel.[25] After 4 h, the reaction was terminated, and the organic layer was separated. After drying over anhydrous sodium sulfate, the solvent was removed under vacuum. The crude product was purified through silica gel chromatography (200–300 mesh) eluted with petroleum ether : ethyl acetate = 6 : 1 (v/v) to give a reddish-brown solid (1.135 g, yield: 82%). ^{1}H NMR (DMSO-d$_6$, 500 MHz) δ (ppm): 5.65 (s, 1H), 5.17 (s, 1H), 4.32 (s, 2H), 2.42 (s, 3H), 2.32 (s, 3H), 2.12 (s, 3H), 1.47 (s, 2H), 0.87(s, 3H). ^{13}C NMR (DMSO-d$_6$, 125 MHz) δ (ppm): 153.28, 139.58, 132.18, 132.03, 129.15, 129.13, 125.37, 121.41, 119.44, 65.48, 17.28, 16.56, 14.01, 11.45. LC-MS (ESI$^+$): *m*/*z* $C_{14}H_{18}BF_2N_3$ calcd 277.1678, found [M + H] 278.1636.

Flow cytometry analysis. The cells were cultured at 2.0×10^5 cells per well in 6-well plates, and then treated with the probe as described above. After harvesting, the cells were washed and suspended in fresh complete medium and analyzed by flow cytometry. The excitation wavelength was selected as 488 nm and the collected emission wavelengths were selected as 500–560 nm.

MTT assay. To assess the potential toxicity of BOD-NH2, MTT assays were carried out. SMMC-7721 cells, HEK293 cells and PC9 cells were placed into 96-well microtiter plates in DMEM with 10% fetal bovine serum (FBS). Then the cells were incubated for 24 h at 37 °C in 5% CO_2/95% air with different concentrations of probe from 0 μM to 80 μM respectively. MTT solution (5.0 mg mL^{-1}, PBS) was then added to each well. After 4 h, the remaining MTT solution was removed. 200 μL of DMSO was added to each well and the plate was shaken for 10 min to dissolve the formazan crystals at room temperature. Absorbance was measured at 570 nm and 630 nm using a TECAN infinite M200pro microplate reader.

Cell imaging. Fluorescence images were acquired on an Olympus FV1000 confocal laser-scanning microscope with an objective lens (×60). The excitation wavelength was chosen as described above. Cells were plated on Petri-dishes (Φ = 20 mm) and allowed to adhere for 24 hours before imaging. The probe was added to the culture plates which were filled with 1 mL fresh complete medium.

Mouse hippocampus imaging. Artificial cerebrospinal fluid (ACSF) was prepared at concentrations of 124 mM NaCl, 2 mM KCl, 1.25 mM KH_2PO_4, 26 mM $NaHCO_3$, 10 mM D-glucose, 2 mM $MgSO_4$, and 2 mM $CaCl_2$. The final pH of the ACSF was 7.4 after saturation with 95% O_2/5% CO_2. The 4–6 week old BALB/c mice were anesthetized with isoflurane in an acrylic desiccator. Brains were removed and placed in a 20 mL dish with ice-cold oxygenated ACSF. The hippocampus was dissected, the superfluous tissue was removed with a small scissor and the brain was transferred for subsequent steps. The thick transverse slices were cut with 300–400 μm at a low speed (3 μm s^{-1}) and a vibration frequency of 70 Hz in ice cold oxygenated ACSF. After transferring these slices into a storage chamber, the slices were rested at RT for at least 1 h prior to staining.

Imaging mice *in vivo*. A Bruker *In vivo* Imaging System was employed to image BALB/c mice. The excitation and emission wavelengths were chosen as described above. The mice were anesthetized prior to injection and during imaging.

Animal testing statement. All surgical procedures were conducted in conformity with the Care and Use of National Guidelines for the laboratory animals, and experimental protocols were approved by the Institutional Animal Care and Use Committee in Binzhou Medical University, Yantai, China. Approval number BZ2014-102R.

Conflicts of interest

There are no conflicts to declare.

Acknowledgements

We acknowledge the National Natural Science Foundation of China (No. 21405172, 21775162, 31470415, 81670064, and 21575159), the program of Youth Innovation Promotion Association, CAS (Grant 2015170), the State Key Laboratory of Environmental Chemistry and Ecotoxicology, Research Center for Eco-Environmental Sciences, CAS (Grant KF2016-22), the Key Laboratory of Sensor Analysis of Tumor Marker Ministry of Education, Qingdao University of Science and Technology (Grant SATM201705), and the Instrument Developing Project of the Chinese Academy of Sciences.

References

1 R. G. Liteplo, R. Beauchamp, M. E. Meek and R. Chenier, *Formaldehyde (Concise International Chemical Assessment Documents)*, World Health Organization, Geneva, 2002.
2 H. Puchtler and S. N. Meloan, *Histochemistry*, 1985, **82**, 201–204.
3 (*a*) T. Salthammer, S. Mentese and R. Marutzky, *Chem. Rev.*, 2010, **110**, 2536–2572; (*b*) K. J. Bruemmer, T. F. Brewer and C. J. Chang, *Curr. Opin. Chem. Biol.*, 2017, **39**, 17–23.
4 (*a*) Y. Shi, F. Lan, C. Matson, P. Mulligan, J. R. Whetstine, P. A. Cole, R. A. Casero and Y. Shi, *Cell*, 2004, **119**, 941–953; (*b*) L. Walport, R. Hopkinson, R. Chowdhury, R. Schiller, W. Ge, A. Kawamura and C. Schofield, *Nat. Commun.*, 2016, **7**, 11974.
5 H. A. Heck, M. Casanova-Schmitz, P. B. Dodd, E. N. Schachter, T. J. Witek and T. Tosun, *Am. Ind. Hyg. Assoc. J.*, 1985, **46**, 1–3.

6 Z. Tong, C. Han, W. Luo, X. Wang, H. Li, H. Luo, J. Zhou, J. Qi and R. He, *Age*, 2013, **35**, 583–596.
7 Z. Tong, W. Luo, Y. Wang, F. Yang, Y. Han, H. Li, H. Luo, B. Duan, T. Xu, Q. Maoying, H. Tan, J. Wang, H. Zhao, F. Liu and Y. Wan, *PLoS One*, 2010, **5**, e10234.
8 T. Nash, *Biochem. J.*, 1953, **55**, 416.
9 E. Janos, J. Balla, E. Tyihak and R. Gaborjanyi, *J. Chromatogr.*, 1980, **191**, 239.
10 S. Kato, P. J. Burke, T. H. Koch and V. M. Bierbaum, *Anal. Chem.*, 2001, **73**, 2992.
11 A. Soman, Y. Qiu and L. Q. Chan, *J. Chromatogr. Sci.*, 2008, **46**, 461–465.
12 (*a*) H. Zhu, J. Fan, J. Du and X. Peng, *Acc. Chem. Res.*, 2016, **49**, 2115–2126; (*b*) X. Li, X. Gao, W. Shi and H. Ma, *Chem. Rev.*, 2014, **114**, 590–659; (*c*) M. Gao, F. Yu, C. Lv, J. Choo and L. Chen, *Chem. Soc. Rev.*, 2017, **46**, 2237–2271; (*d*) F. Yu, X. Han and L. Chen, *Chem. Commun.*, 2014, **50**, 12234; (*e*) X. Han, F. Yu, X. Song and L. Chen, *Chem. Sci.*, 2017, **8**, 6991–7002; (*f*) S. Li, Z. Sun, R. Li, M. Dong, L. Zhang, W. Qi, X. Zhang and H. Wang, *Sci. Rep.*, 2015, **5**, 8475; (*g*) Z. Sun, S. Li, Y. Jiang, Y. Qiao, L. Zhang, L. Xu, J. Liu, W. Qi and H. Wang, *Sci. Rep.*, 2016, **6**, 20553; (*h*) M. Dong, C. Liu, S. Li, R. Li, Y. Qiao, L. Zhang, W. Wei, W. Qi and H. Wang, *Sens. Actuators, B*, 2016, **232**, 234–242; (*i*) N. Zhang, Y. Si, Z. Sun, L. Chen, R. Li, Y. Qiao and H. Wang, *Anal. Chem.*, 2014, **86**, 11714.
13 (*a*) M. Tian, X. Peng, F. Feng, S. Meng, J. Fan and S. Sun, *Dyes Pigm.*, 2009, **81**, 58–62; (*b*) X. Han, F. Yu, X. Song and L. Chen, *Adv. Funct. Mater.*, 2017, **1700769**, 1–9; (*c*) F. Yu, M. Gao, M. Li and L. Chen, *Biomaterials*, 2015, **63**, 93–101; (*d*) X. Chen, T. Leng, C. Wang, Y. Shen and W. Zhu, *Dyes Pigm.*, 2017, **141**, 299–305; (*e*) X. Han, F. Yu, X. Song and L. Chen, *Chem. Sci.*, 2016, **7**, 5098–5107.
14 K. J. Bruemmer, T. F. Brewer and C. J. Chang, *Curr. Opin. Chem. Biol.*, 2017, **39**, 17–23.
15 (*a*) T. F. Brewer and C. J. Chang, *J. Am. Chem. Soc.*, 2015, **137**, 10886–10889; (*b*) A. Roth, H. Li, C. Anorma and J. Chan, *J. Am. Chem. Soc.*, 2015, **137**, 10890–10893; (*c*) K. J. Bruemmer, R. R. Walvoord, T. F. Brewer, G. Burgos-Barragan, N. Wit, L. B. Pontel, K. J. Patel and C. J. Chang, *J. Am. Chem. Soc.*, 2017, **139**, 5338–5350; (*d*) T. F. Brewer, G. Burgos-Barragan, N. Wit, K. J. Patel and C. J. Chang, *Chem. Sci.*, 2017, **8**, 4073–4081; (*e*) L. He, X. Yang, Y. Liu, X. Kong and W. Lin, *Chem. Commun.*, 2016, **52**, 4029–4032; (*f*) J. Xu, Y. Zhang, L. Zeng, J. Liu, J. M. Kinsella and R. Sheng, *Talanta*, 2016, **160**, 645–652; (*g*) J. B. Li, Q. Q. Wang, L. Yuan, Y. X. Wu, X. X. Hu, X. B. Zhang and W. Tan, *Analyst*, 2016, **141**, 3395–3402; (*h*) S. Singha, Y. W. Jun, J. Bae and K. H. Ahn, *Anal. Chem.*, 2017, **89**, 3724–3731; (*i*) X. Xie, F. Tang, X. Shangguan, S. Che, J. Niu, Y. Xiao, X. Wang and B. Tang, *Chem. Commun.*, 2017, **53**, 6520–6523; (*j*) Z. Li, Y. Xu, H. Zhu and Y. Qian, *Chem. Sci.*, 2017, **8**, 5616–5621; (*k*) Z. Xie, J. Ge, H. Zhang, T. Bai, S. He, J. Ling, H. Sun and Q. Zhu, *Sens. Actuators, B*, 2017, **241**, 1050–1056; (*l*) K. Dou, G. Chen, F. Yu, Y. Liu, L. Chen, Z. Cao, T. Chen, Y. Li and J. You, *Chem. Sci.*, 2017, **8**, 7851–7861.
16 (*a*) Y. Tang, X. Kong, A. Xu, B. Dong and W. Lin, *Angew. Chem., Int. Ed.*, 2016, **55**, 3356–3359; (*b*) Y. Tang, X. Kong, Z. R. Liu, A. Xu and W. Lin, *Anal. Chem.*, 2016, **88**, 9359–9363; (*c*) Y. H. Lee, Y. Tang, P. Verwilst, W. Lin and J. S. Kim, *Chem. Commun.*, 2016, **52**, 11247–11250; (*d*) C. Liu, C. Shi, H. Li, W. Du, Z. Li, L. Wei and M. Yu, *Sens. Actuators, B*, 2015, **219**, 185–191; (*e*) X. Liang, B. Chen, L. Shao, J. Cheng, M. Huang, Y. Chen, Y. Hu, Y. Han, F. Han and X. Li, *Theranostics*, 2017, **7**, 2305–2313; (*f*) Y. Tang, Y. Ma, A. Xu, G. Xu and W. Lin, *Methods Appl. Fluoresc.*, 2017, **5**, 024005.
17 C. Liu, X. Jiao, S. He, L. Zhao and X. Zeng, *Dyes Pigm.*, 2017, **138**, 23–29.
18 (*a*) F. Yu, P. Li, B. Wang and K. Han, *J. Am. Chem. Soc.*, 2013, **135**, 7674–7680; (*b*) A. Kaur, J. L. Kolanowski and E. J. New, *Angew. Chem., Int. Ed.*, 2016, **55**, 1602–1613; (*c*) Z. Lou, P. Li and K. Han, *Acc. Chem. Res.*, 2015, **48**, 1358–1368; (*d*) F. Yu, P. Song, P. Li, B. Wang and K. Han, *Chem. Commun.*, 2012, **48**, 7735–7737.
19 (*a*) P. Liu, X. Jing, F. Yu, C. Lv and L. Chen, *Analyst*, 2015, **140**, 4576–4583; (*b*) M. Gao, R. Wang, F. Yu, J. You and L. Chen, *Analyst*, 2015, **140**, 3766–3772.
20 Y. Oshikawa and A. Ojida, *Chem. Commun.*, 2013, **49**, 1373–1375.
21 (*a*) J. Wu, W. Liu, J. Ge, H. Zhang and P. Wang, *Chem. Soc. Rev.*, 2011, **40**, 3483–3495; (*b*) Y. Sun, P. Wang, J. Liu, J. Zhang and W. Guo, *Analyst*, 2012, **137**, 3430–3433; (*c*) J. S. Wu, W. M. Liu, X. Q. Zhuang, F. Wang, P. Wang, S. Tao, X. Zhang, S. K. Wu and S. T. Lee, *Org. Lett.*, 2007, **9**, 33–36; (*d*) G. J. Zhao and K. L. Han, *Acc. Chem. Res.*, 2012, **45**, 404–413.
22 (*a*) W. Tsai, T. T. Nguyen, Y. Shi and M. C. Barton, *Mol. Cell. Biol.*, 2008, **28**, 5139–5146; (*b*) C. Binda, S. Valente, M. Romanenghi, S. Pilotto, R. Cirilli, A. Karytinos, G. Ciossani, O. A. Botrugno, F. Forneris, M. Tardugno, D. E. Edmondson, S. Minucci, A. Mattevi and A. Mai, *J. Am. Chem. Soc.*, 2010, **132**, 6827–6833; (*c*) J. C. Culhane, L. M. Szewczuk, X. Liu, G. Da, R. Marmorstein and P. A. Cole, *J. Am. Chem. Soc.*, 2006, **128**, 4536–4537.
23 (*a*) K. Tulpule and R. Dringen, *J. Neurochem.*, 2013, **127**, 7–21; (*b*) W. S. Bosan, C. E. Lambert and R. C. Shank, *Carclnogenesis*, 1986, **7**, 413–418; (*c*) J. R. Ridpath, A. Nakamura, K. Tano, A. M. Luke, E. Sonoda, H. Arakawa, J. M. Buerstedde, D. A. Gillespie, J. E. Sale, M. Yamazoe, D. K. Bishop, M. Takata, S. Takeda, M. Watanabe, J. A. Swenberg and J. Nakamura, *Cancer Res.*, 2007, **67**, 11117–11122; (*d*) T. Rétfalvi, Z. I. Németh, I. Sarudi and L. Albert, *Acta Biol. Hung.*, 1998, **49**, 375–379.
24 P. Rivera-Fuentes, A. T. Wrobel, M. L. Zastrow, M. Khan, J. Georgiou, T. T. Luyben, J. C. Roder, K. Okamoto and S. J. Lippard, *Chem. Sci.*, 2015, **6**, 1944–1948.
25 (*a*) B. Tang, F. Yu, P. Li, L. Tong, X. Duan, T. Xie and X. Wang, *J. Am. Chem. Soc.*, 2009, **131**, 3016–3023; (*b*) S. Uchiyama, T. Tsuji, K. Ikado, A. Yoshida, K. Kawamoto, T. Hayashi and N. Inada, *Analyst*, 2015, **140**, 4498–4506.